Response to the comments by Reviewer #1

Thank Reviewer #1 for very valuable comments on my manuscript. The revisions are marked with red. My answers to your comments are given below:

1. Among the physical models to approach earthquake faults, the single spring-slider model, which can represent a single fault, is actually the simplest one. However, based on this simple model in the presence of thermal-pressurized friction and viscosity we can obtain good simulations of earthquake recurrences along a single fault. Results can exhibit the frictional and viscous effects on earthquake recurrence.
2. The statements "Because … " in Line 239 will be re-written to be "Figures show that the maximum values of both V and U decrease from case (a) to case (d) in each figure. Hence, the maximum velocity and maximum displacement, which are denoted by V_{max} and U_{max}, respectively, for case (a) can be taken as the scaled factor to normalize the waveforms from case (a) to case (d). This makes us easily to compare the waveforms of the four cases in each figure."
3. The statements to show the weak points of the single spring-slider model and the improvement on English writing for the manuscript will be made after I receive the comments by other reviewers.

Response to the Comments by Reviewer #2

Review of the paper "A Study of Earthquake Recurrence based on a One-body Spring-slider Model in the Presence of Thermal-pressurized Slip-weakening Friction and Viscosity" by Jeen-Hwa Wang

This paper studied earthquake recurrence by numerical simulations of a one-degree-of-freedom spring-slider model with thermal-pressurized slip-weakening friction. The paper investigated the effects of the viscosity and the wear process on the recurrence time, slip amount for each event, slip velocity, and so on.

The many parts of the main results stated in the manuscript would not be obtained or read from the simulation results shown in Figs. 4-12. The main reasons of this were the assumption of the constant U_c in the simulations for the examination of the wear effect (Figs. 8-12) and the way of drawing Figs. 4-12.

Regarding the following specific comments [1]-[6] at least, the numerical simulations should be conducted appropriately and the manuscript and figures should be modified before the publication.

[Answer] I would like to express my thanks to you for carefully reading my manuscript and giving me many valuable comments and suggestions to improve the manuscript. The revisions are marked with red.

Major comments

[1] L.23-28 (Abstract), L.385, etc.: The Author stated that the effect of the wear process increases with C. However, the dependency of C on T_R or D is not obtained from the simulation results shown in Figs. 8-12. This is because U_c was assumed to be constant and the same in (a)-(d) for each figure, as stated in L.266-269 and captions of Figs. 8-12, which means that the other parameters (at least one among ρ_f, C_v, μ_f, Λ, and D_0) varied with C in (a)-(d) for each figure. In order to investigate the effect of C solely, the other parameters (ρ_f, C_v, μ_f, Λ, and D_0) should be constant and the same in (a)-(d), and thus U_c should change in (a)-(d) and vary with h(t) (i.e., the cumulated slip). It is better to calculate U_c using h=CS(t) for every time step in the simulations.

[Answer] Actually, U_c is not constant and varies with h in panels (a)–(d) of Figs. 8–12. The value of U_c written in each figure caption is the initial value, U_{co}, in the relationship: $U_c=U_{co}+C\Sigma U$ assumed by me. This point has been explained in the revised manuscript. The re-written statements are "Simulation results for four values of C are shown in Figs. 8–12: (a) for C=0.0001; (b) for C=0.001; (c) for C=0.01; and (d) for C=0.05 when η=0 in Figs. 8–10 and when η=1 in Figs. 11–12. The initial values of U_c are 0.1 for Fig. 8, 0.5 for Fig. 9, 0.9 for Fig. 10, 0.1 for Fig. 11, and 0.5 for Fig. 12." Meanwhile, the value of U_c shown in each figure caption has been replaced by "U_{co}."

[2] ・L.285-286: "The left-handed-side panels in Figs. 5–7 show that V_m and D decrease when … U_c … increases"

・L.290-293

・L.309-310: "The phase portraits shown in the right-handed-side panels of Figs. 5–7 exhibit that … the size associated with D decrease with increasing η."

The values of V_m, D, and the slope at the two fixed points cannot be compared among Figs.

5-7 because V and U would be normalized by different values of V_{max} and U_{max} among the figures. I guessed that V_{max} and U_{max} correspond to the maximum values of V and U in (a) for each figure and that the maximum values decreases with increasing U_c when $\eta \neq 0$, similar to the cases with $\eta=0$ (Fig. 4). I suggest that V and U should be normalized by V_p and $V_p\tau_{max}$, respectively, where τ_{max} is the maximum value of the horizontal axis (1300) in Figs. 4-12.
[Answer] It is very sorry that the notations were not well explained in the original manuscript. The values of V_m and D, respectively, represent the peak value of velocity and final slip of an event in each figure and have been displayed in Fig. 1 which has been re-drawn and different from the original one. The quantities V_{max} and U_{max} are the maximum values of V and U, respectively, in the first panel marked by "a" of a figure with four panels. The normalization scales in the left-handed-side panels of Figs. 4–12 are V_{max} for the velocities and the final value of $\Sigma U/U_{max}$ for the cumulative displacements in the computational time. Hence, the upper bound scales are "1" for both the velocity and the displacement. Hence, only the patterns of temporal variations of velocity and cumulative slip are concerned in these figures. The above-mentioned explanations have been added to the revised manuscript

[3] ・L.17-18: "T_R increases when U_c decreases or η increases"

・L.286-287: "T_R increases when either η increases or U_c decreases"

T_R increases when η increases for U_c=0.8 (Fig. 7), while T_R decreases when η increases for smaller U_c (Figs. 5 and 6). The behaviors of stick-slips should be investigated more carefully.
[Answer] The related description has been improved.

[4] ・L.276-277: "The value of τ_D increases with U_c"

・L.286: "while τ_D increases with η and U_C"

The τ_D values are unclear in the left panels of Figs. 4-6. Please add the enlarged figures for only one event.
[Answer] Figure 1 has been re-drawn to include the temporal variation in particle velocity to meet your request.

[5] L. 278-282, L.288-292, L.405-407: I cannot understand what "the slope values at the two fixed points" means

$(V/V_{max})/(U/U_{max})$? Or $\frac{U_{max}}{V_{max}} \frac{dV}{dU}$?

[Answer] The slope means $d(V/V_{max})/d(U/U_{max})=(U_{max}/V_{max})(dV/dU)$. This statement has been added to the revised manuscript. By the way, the term "the slope value" has been replaced by "the absolute value of slope" in the revised manuscript.

[6] Some characters in the numerical formulas are very confusing.

- About slip and cumulative slip
  - u and U in the friction law (equation 2, the second term of the right side of equations 3 and 4, Figure 3, etc.) would represent the time-varying slip amount for one event.
  - u and U in $u-u_0$ and $U-V_p\tau$ (the first term of the right side of equations 1, 3, and 4, Figure 1, etc.) show the time-varying cumulative slip.
  - Also ΣU in Figs.4-12 correspond to the time-varying cumulative slip.
  - The (maybe time-varying) cumulative slip used in the wear effect is S(t). Is S(t) the same as ΣU in Figs.4-12?
  - Is D(t) in S(t)=ΣD(t) different from D (final slip of each event, defined at L.16)?

  [Answer] The u and U only represent the time-varying slip and time-varying normalized slip, respectively, for one event and they do not denote the time-varying cumulative slip. The parameter ΣU represents the time-varying cumulative slip. D(t), which represents the final slip of an event, could be constant in the time history as displayed in Figs. 4–7 when all model parameters do not change with time; while it could vary with time as shown in Figs. 8–12 when one of the model parameters does change with time. Hence, D(t) in S(t)=ΣD(t) is merely D. This point has been explained in the revised manuscript.

- About friction, is *f* in L.155 the same as μ_f (L.156 etc.)?

  [Answer] The "*f*" in L.155 has been replaced by "μ_f".

<u>Minor comments</u>

[7] The topic on the wear process starts abruptly at L.20 in Abstract and the last paragraph of Section 4 (Simulation Results, p.11). To clarify the subjects of this paper, it would be better to add the statement that this paper investigated the wear process to the first sentence in Abstract and to the Introduction. In addition, the statements on the wear process in p.11 should be moved to somewhere before Section 4.
[Answer] The statement "the wear process" has been moved to the places you suggested in the revised manuscript

[8] L.53: 'the Nankaido trough' → 'the Nankaido segment of the Nankai Trough'?
[Answer] The statement has been re-written in the revised manuscript.

[9] "$T_R=\Delta\sigma^{2/3}M_o^{1/3}/1.81\mu v_l$ ": The assumption of constant Δσ and v_l is not needed to derive this relation. If Δσ or v_l varies with time, also T_R varies with time.
[Answer] The related statement has been deleted in the revised manuscript.

[10]L.71-72: I cannot understand the meaning of 'the distribution of T_R'. The probability density distribution of T_R?
[Answer] Yes, you are right. It is the probability density distribution of T_R. The related statement has been added in the revised manuscript

[11]L.87: 'the Nankaido trough' → 'the Nankai trough'? Or 'the Nankaido segment of the Nankai Trough'?
[Answer] The statement "the Nankaido trough" has been replaced by "the Nankai trough" in the revised manuscript.

[12]L.152-153: "The latter is not appropriate in this study because of the request of constant velocity. " The equations of SOP model for variable velocity are shown in Rice (2006), which can be solved numerically. It should be noted that I agree to adopt AUD model in this study in order to examine the wear effect.
[Answer] The statement has been re-written in the revised manuscript.

[13]L.163 (equation 2): How did the Author treat equation 2 for the stable sliding (e.g. cases shown in Figs. 11d and 12d)? u=0?
[Answer] The value of F(u) at u=0 if F_o, i.e., the static friction force. The statement has been re-written in the revised manuscript.

[14] ・L.167-168: "The force drop is lower for larger u_c than for smaller u_c."

・L.399: "larger U_c yields a lower ΔF than smaller U_c"

The final friction drop is 1, regardless of u_c and U_c (Fig. 3). Did the Author mean "the force drop for a certain displacement"?
[Answer] You are right. The statement "for the same final slip" has been added to the revised manuscript.

[15]p.8: υ decreases with increasing T and η is proportional to υ. However, η was assumed to be constant in this study. I wonder if the simulations with η depending on T are possible. The Author does not have to conduct such simulations in this study, but the comments on this may be interesting.
[Answer] The statements "Since υ decreases with increasing T, η decreases with increasing T. Hence, η can vary with time during faulting. This point has been studied by Wang (2017b) for the generation of nuclear phase before an earthquake ruptures. In this study, constant η is considered for each case" have been added to the revised manuscript.

[16]L.222: "V_p must be much smaller than 1": The value of V_p depends on $D_o\omega_o$. How large is $D_o\omega_o$?
[Answer] In this study, is considered to be about 1 m/s.

[17]L.223: "V_p is taken to be 10^{-2}" Do the results change if V_p is another value?
[Answer] The statements "Since the value of V_p can only influence the recurrence time, T_R, between two events and cannot influence the pattern of time variations in velocities and displacements of events. In order to study earthquake recurrence, there must be numerous modelled events with clear and visualized time functions of displacements and velocities for an event in the computational time period. If $V_p=10^{-10}$ is considered, T_R is very long and thus τ_D is much shorter than T_R. This makes the time function of an event displayed in the

variation in slip looks like a step function for the displacements and an impulse for the velocities. Hence, V_p=10^{-2} is taken in this study."

[18] Section 4 (Simulation Results): The results of the numerical simulations stated in pp.12-13 and L.381-414 should be moved to Section 4.
[Answer] The related statements shown in the section of "Discussion" have been moved to the section of "Simulation Results".

[19] L.252-253: The references are needed.
[Answer] The related references have been added to the revised manuscript.

[20] L.264-265, L.377-378 etc.: "U_c is proportional to C": This phrase seems to be strange for me because the variable is S(t) and C is the proportion coefficient.
[Answer] The statements have been re-written in the revised manuscript.

[21] L.265: "This": What does the word "this" show? The sentence just before this word? The fact "the more mature the fault is, the thicker its slip zone is" comes only from h(t)=CS(t).
[Answer] The sentence has been re-written as "Based on *h(t)=CS(t)*, the more mature the fault is, the thicker its slip zone is." in the revised manuscript.

[22] L.274-276: "the force drop, ΔF, decreases with increasing U_c, thus indicating that larger ΔF yields higher V_m and larger D" I cannot understand the logic of this sentence. The Author's intention may be "ΔF decreases with increasing U_c for a certain finite displacement" because the friction drop reaches 1 when displacement is ∞ regardless of U_c (Fig.3). If so, however, this phrase have no relation to "larger ΔF yields larger D".
[Answer] The statement "" has been behind the sentence in the revised manuscript.

[23] L.292-293: The U_c values are different from those in L.248 and figure captions.
[Answer] The values of Uc shown in L.292-293 are wrong and must the same as those in L.248. The original sentence has been re-written to be "Clearly, like Fig. 4 the final slip decreases with increasing U_c."

[24] L.301-305: In a one-degree-of-freedom spring-slider model with constant friction parameters, the system reaches limiting cycles even in the previous studies listed in L.304-305, although I have not checked the results by Kostić et al. (2013a) and Franović et al. (2016). The Author may consider the initial transient phase, but the phase depends on the assumed initial state before the spring starts to be pull with the driving velocity of V_p. The behaviors of the limiting cycle reflect the parameters of the friction and of the system properly. It should be noted that the very small transient phase was also observed in Rice and Tse (1986) (the reference in L.298).
[Answer] Your viewpoint is correct. In this study, I mainly focus on the effect on recurrence. The phase portrait is just used to express the possible change of fixed points due to either a use of different values of or a use of time-varying values of model parameters. Nonlinear behavior, including very small transient phase which was not observed in this study, of the system will be my next study.

[25] L.309-310: I cannot understand that the right panels show T_R.
[Answer] The related statements have been deleted in the revised manuscript.

[26]L.314: I cannot understand why larger η generates chaos.
[Answer] The word "chaos" has been re-written as "an attractor" in the revised manuscript.

[27]L.318: The slope values at V=0 and U=0 decrease with increasing η more drastically for the larger U_c. As pointed out in my comment [2], the slope values should not be compared among the figures because U_{max} and V_{max} values are different among the figures.
[Answer] As mentioned in my answer of your comment [2], for a certain figure we can the absolute values of slope in the four right-handed-sides panels because their values of V_{max} and U_{max} are the same. Of course, it is not good to compare the values in different figures due to different values of V_{max} and U_{max} in use.

[28]L.319: The references are needed.
[Answer] "The previous study" means the simulation results of this study. Hence, the words "The previous study" have been re-written as "The simulation results as mentioned previously".

[29]L.321: "the effects" The effects of temporal variations of η and U_c?
[Answer] The following statement "the effects of time-dependent η and U_c" has been added to the revised manuscript.

[30]L.329-330: "$\Lambda=(\lambda_f-\lambda_n)/(\beta_f+\beta_n)$"
It would be better to move this to p.7, adding the definition of λ_f, λ_n, β_f, and β_n.
[Answer] The statements have been re-written and added in the revised manuscript.

[31]L.338: "$\mathrm{\mu_f}$" → "μ_f"
[Answer] "$\mathrm{\mu_f}$" is replaced by "μ_f" in the revised manuscript.

[32]L.347: "$\mathrm{\rho_f}$" and "n" → "ρ_f" and "*n*"
[Answer] "$\mathrm{\rho_f}$" and "n" are replaced, respectively, by "ρ_f" and "*n*" in the revised manuscript.

[33]L.362-364: The Author used the words "time-varying". However, "the increase in permeability can result in the increase in pore pressure due to slip" would be better because "This" in the sentence "This can reduce the frictional resistance" obviously means an increase in the pore pressure.
[Answer] The statement "The time-varying permeability can result in the time-varying pore pressure, p_f" has been re-written as "An increase in permeability can result in an increase in pore pressure, p_f".

[34]L. 410: "C" → "*C*"?
[Answer] "C" is replaced by "*C*" in the revised manuscript.

[35]L.411: "approaches unity" The slope values seem to become smaller than unity in Figs. 9-12. Plotting the slope values (with time or slip) may clarify this point.
Why does the unity important? The slope values depend on the V_{max} and U_{max} values.

[Answer] Actually, the slope values become smaller than unity in Figs. 9-12. Hence, the statement "approach to unity" has been deleted in the revised manuscript.

[36] Bizzarri (2010) showed the effects of the wear process on the stick-slip behaviors, assuming the friction law with thermal pressurization, and thus the results on the wear processes in this study are not new. I suggest that the statements on the results of the simulations including both the wear processes and the viscous effects (Figs. 11 and 12) are added.
[Answer] I agree with you. Related information has been added to the revised manuscript.

[37] Are the η and C values used in the simulations consistent with those estimated by observations or laboratory experiments in previous studies (e.g., Boneh et al., 2014, pageoph)?
[Answer] This study is merely my first step to theoretically explore the earthquake recurrences caused by time-varying model parameters through numerical simulations. In this study, I just want to theoretical explore the possible effects on earthquake recurrences caused by time-varying of fault width. Hence, only the assumed values have been taken into account. I have not yet compared my values with those obtained by others. I will approach the problem for real faults in near future, and thus it is necessary to take the values of model parameters obtained from field observations and laboratory experiments into account.

[38] Vertical aces in Figs. 4-12: Please add the scales of the $\Sigma U/U_{max}$ aces. The maximum of $\Sigma U/U_{max}$ must be larger than 1 because U/U_{max} reaches 1 or larger in the right panels of (a).
[Answer] In Figs. 8–12, the velocity waveforms and displacements are normalized by the maximum values of each figure. Hence, the upper bound value of the vertical axis is 1. The statements have been added to the revised manuscript.

[39] Fig.8-12: Why do the behaviors of the stick-slips (e.g., T_R, D, and V_m) vary with time in spite of the constant U_c?
[Answer] The values of U_c are not constant and vary with time in Figs. 8–12. The values of U_c shown in the text and figure captions of have been re-written to be the initial values of U_c.

[40] Figs.11(a) and 12(a): Why $V_m/V_{max} \neq 1$? I guessed that V_{max} was defined as V_m in (a) for each figure in Figs. 4-10. Why is the maximum of U/U_{max} larger than 1? I guessed that U_{max} was defined as the maximum of U in each figure in Figs. 4-10.
[Answer] It is very sorry that the numerical computation cannot work when C is larger than a certain value which depends on U_c. The normalization of original Fig. 11 and Fig 12 was made based on the maximum values of panel (d), which are wrong. The re-computed results are displayed in the revised manuscript.

[41] Figs. 11(d) and 12(d): Why are there two thin solid lines? Why is $\Sigma U/U_{max}$ constant (thick solid line)?
[Answer] It is very sorry that the numerical computation cannot work when C is

larger than a certain value. Originally, I kept the bad simulation results for C=0.05 in Figs. 11–12 with η=1, because I wanted to retain the same four values of C for Figs. 8–12. This idea sounds not good. Hence, I have re-done the numerical computations to find out the upper bound value of C for a certain U_c with η=1. The re-computed results are displayed in Figs. 11–12 of the revised manuscript.

A Study of Earthquake Recurrence based on a One-body Spring-slider Model in the Presence of Thermal-pressurized Slip-weakening Friction and Viscosity

Jeen-Hwa Wang

Institute of Earth Sciences, Academia Sinica, P.O. Box 1-55, Nangang, Taipei, TAIWAN (e-mail: jhwang@earth.sinica.edu.tw)

(submitted to Natural Hazards and Earth System Sciences on December 29, 2017; re-submitted on January 18, 2018; revised on June 4, 2018)

Abstract Earthquake recurrence is studied from the temporal variation in slip through numerical simulations based on the normalized form of equation of motion of a one-body spring-slider model with thermal-pressurized slip-weakening friction and viscosity. The wear process, whose effect is included in the friction law, is also taken into account in this study. The main parameters are the normalized characteristic displacement, U_c, of the friction law and the normalized damping coefficient (to represent viscosity), η. Define T_R, D, and τ_D to be the recurrence time of events, the final slip of an event, and the duration time of an event, respectively. Simulation results show that T_R increases when U_c decreases or η increases; D and τ_D decrease with increasing η; and τ_D increases with U_c. The time- and slip-predictable model can describe the temporal variation in cumulative slip. When the wear process is considered, the thickness of slip zone, h which depends on the cumulated slip, $S(t)=\sum D(t)$, i.e., $h(t)=CS(t)$ (C=a dimensionless increasing rate of h with S) is an important parameter influencing T_R and D. U_c is a function of h and thus depends on cumulated slip, $\sum U$, with an increasing rate of C. In the computational time period, the wear process influences the recurrence of events and such an effect increases with C when C>0.0001. When viscosity is present, the effect due to wear process becomes stronger. Both T_R and D decrease when the fault becomes more mature, thus suggesting that it is more difficult to produce large earthquakes along a fault when it becomes more mature. Neither the time-predictable model nor the slip-predictable one can describe the temporal variation in cumulative slip of earthquakes under the wear process with large C.

Key Words: Recurrence of earthquakes, final slip, rise time, one-body spring-slider model, thermal-pressurized slip-weakening friction, characteristic displacement, viscosity, wear process

1 Introduction

Earthquake recurrence that is relevant to the physics of faulting is an important factor in seismic hazard assessment. It is related to the seismic cycle, which represents the occurrence of several earthquakes in the same segment of a fault during a time period. Fig. 1 exhibits the general pattern of time variation in slip and particle velocity during a seismic cycle. In the figure, T_R is the recurrence (also denoted by repeat or inter-event) time of two events in a seismic cycle, τ_D is the duration time of slip of an event, D is the final slip of an event, and V_m is the peak value of particle velocity of an event. The four parameters could be constants in the time history when all model parameters do not vary with time and could also vary with time, represented by $T_R(t)$, $\tau_D(t)$, $D(t)$, and $V_m(t)$, when one of model parameters does vary with time. Sykes and Quittmeyer (1981) pointed out that the major factors in controlling T_R are the plate moving speed and the geometry of the rupture zone. Based on Reid's elastic rebound theory (Reid, 1910), Schwartz and Coppersmith (1984) assumed that an earthquake occurs when the tectonic shear stress on a fault is higher than a critical level, which is dependent on the physical conditions of the fault and the loading by regional tectonics. Since in their work a fault has a homogeneous distribution of physical properties under constant tectonic loading, earthquakes could happen regularly.

Some observations exhibit periodicity for different size earthquakes. Bakun and McEvilly (1979) obtained $T_R \approx 23 \pm 9$ years for M≈6 earthquakes at the Parkfield segment of the San Andreas fault, USA since 1857. Sykes and Menke (2006) estimated $T_R \approx 100$ years for $M \geq 8$ earthquakes in the Nankaido segments of the Nankai trough, Japan. Okada et al. (2003) gained $T_R = 5.5 \pm 0.7$ years for earthquakes with $M = 4.8 \pm 0.1$ off Kamaishi, Japan, since 1957. Nadeau and Johnson (1998) inferred an empirical relation between T_R and seismic moment, M_o: $T_R \propto M_o^{1/6}$. To make this relation valid, the stress drop, $\Delta\sigma$, or the long-term slip velocity of a fault, v_l, must be in terms of M_o. Based on three data set from eastern Taiwan, Parkfield, USA, and northeastern Japan, Chen et al. (2007) inferred $T_R \sim M_o^{0.61}$. Beeler et al. (2001) proposed a theoretical relation: $T_R = \Delta\sigma^{2/3} M_o^{1/3} / 1.81 \mu v_l$, where μ is the rigidity of the fault-zone materials.

However, the main factors in influencing earthquake occurrences commonly are spatially heterogeneous and also vary with time. Thus, the recurrence times of earthquakes, especially large events, are not constant inferred either from observations (Ando, 1975; Sieh, 1981; Kanamori and Allen, 1986; Wang and Kuo, 1998; Wang, 2005; Sieh et al., 2008) or from modeling (Wang, 1995, 1996; Ward, 1996, 2000; Wang and Hwang, 2001). Kanamori and Allen (1986) observed that faults with longer T_R are stronger than those with shorter T_R. Davies et al. (1989) proposed that the longer it has been since the last earthquake, the longer the expected time till the next. Wang and Kuo (1998) observed that for $M \geq 7$ earthquakes in Taiwan T_R strongly follows the Poissonian processes. Enescu et al. (2008) found that the probability density distribution of T_R can be described by an exponential function. From the estimated values of T_R of earthquakes happened on the Chelungpu fault in central Taiwan from trenching data, Wang (2005) found that the earthquakes occurred non-periodically.

In order to interpret earthquake recurrences, Shimazaki and Nakata (1980) proposed three simple phenomenological models. Each model has a constantly increasing tectonic stress that is controlled by a critical stress level, σ_c, for failure and a base stress level, σ_b. The three models are: (1) the perfectly periodic model (with constant σ_c, σ_b, and $\Delta\sigma$); (2) the time-predictable model (with constant σ_c, variable σ_b, and variable $\Delta\sigma$); and (3) the slip-predictable model (with variable σ_c, constant σ_b, and variable $\Delta\sigma$). For the first model, both T_R and D of next earthquake can be predicted from the values of T_R or D of previous ones. For the second model, T_R of next earthquake can be predicted from the values of D of previous ones. For the third model, D of next earthquake can be predicted from the values of T_R of previous ones. However, debates about the three models have been made for a long time. Some examples are given below. Ando (1975) suggested that the second model worked for post-1707 events, yet not for pre-1707 ones in the Nankai trough, Japan. Wang (2005) assumed that the second model could describe the earthquakes occurred on the Chelungpu fault, Taiwan in the past 1900 years. For the Parkfield earthquake sequence, Bakun and McEvilly (1984) took different models; while Murray and Segall (2002) considered the failure of the second model. From laboratory results, Rubinstein et al. (2012) assumed the failure of the time- and slip-predictable models for earthquakes.

Some models, for instance the crack model and dynamical spring-slider model, have been developed for fault dynamics, even though the seismologists have not a comprehensive model. There are several factors in controlling fault dynamics and earthquake ruptures (see Bizzarri, 2009; Wang, 2017b). Among the factors, friction (Nur, 1978; Belardinelli and Belardinelli, 1996) and viscosity (Jeffreys, 1942; Spray, 1993; Wang, 2007) are two significant ones.

Modeling earthquake recurrence based on different models has been long made and is reviewed by Bizzarri (2012a,b) and Franović et al. (2016). Among the models, the spring-slider model has been used to study fault dynamics and earthquake physics (see Wang 2008). Burridge and Knopoff (1967) proposed the one-dimensional N-body model (abbreviated as the 1-D BK model henceforth). Wang (2000, 2012) extended the 1-D model to 2-D one. The one-, two-, three-, and few-body models with various friction laws have also been applied to approach fault dynamics (see Turcotte, 1992). The studies for various friction laws based on spring-slider models are briefly described below: (1) for rate- and state-dependent friction (e.g., Rice and Tse, 1986; Ryabov and Ito, 2001; Erickson et al., 2008, 2011; He et al., 2003; Mitsui and Hirahara, 2009; Bizzarri, 2012a; Abe and Kato, 2013;Kostić et al., 2013a; Bizzarri and Crupi, 2014; Franović et al., 2016); (2) for velocity-weakening friction (e.g., Carlson and Langer, 1989; Huang and Turcotte, 1992; Brun and Gomez, 1994; Wang and Hwang, 2001; Wang, 2003; Kostić et al., 2013b); (3) for simple static/dynamic friction (e.g., Abaimov et al., 2007; Hasumi, 2007).

Some results concerning earthquake recurrence are simply explained below. Erickson et al. (2008) suggested that aperiodicity in earthquake dynamics is due to either the nonlinear friction law (Huang and Turcotte, 1990) or the heterogeneous stress distribution (Lapusta and Rice, 2003). Wang and Hwang (2001) emphasized the importance of heterogeneous frictional strengths. Mitsui and Hirahara (2009) pointed out the effect of thermal pressurization. Dragoni and Piombo (2011) found that variable strain rate causes aperiodicity of earthquakes. Bizzarri and Crupi (2014) found that T_R is dependent on the loading rate, effective normal stress, and characteristic distance of the rate- and state-dependent friction law.

As mentioned previously, numerous studies have been made for exploring the frictional effect on earthquake recurrence. But, the study concerning the viscous effect on earthquake recurrence is rare. In the followings, we will investigate the effects of slip-weakening friction due to thermal-pressurization and viscosity on earthquake recurrence based on the one-body spring-slider model.

2 One-body Model

Fig. 2 displays the one-body spring-slider model. In the model, m, K, N, F, η, u, v ($=du/dt$), v_p, and $u_o=v_pt$ denote, respectively, the mass of the slider, the stiffness (or spring constant) of the leaf spring, the normal force, the frictional force between the slider and the moving plate, the damping coefficient (to represent viscosity as explained below), the displacement of the slider, the velocity of the slider, the plate moving speed, and the equilibrium location of the slider. The frictional force F (with the static value of F_o) is usually a function of u or v. Viscosity results in the viscous force, Φ, between the slider and the moving plate, and Φ is in terms of v. A driving force, Kv_pt, caused by the moving plate through the leaf spring pulls the slider to move. The equation of motion of the model is:

$$md^2u/dt^2=-K(u-u_o)-F(u,v)-\Phi(v). \quad (1)$$

When $Kv_pt \geq F_o$, F changes from static frictional force to dynamic one and thus makes the slider move. Among the physical models to approach earthquake faults, the single spring-slider model, which can represent a single fault, is actually the simplest one. However, based on this simple model in the presence of thermal-pressurized friction and viscosity we can obtain good simulations of earthquake recurrences along a single fault. Results can exhibit the frictional and viscous effects on earthquake recurrence.

The frictional force $F(u,v)$ is controlled by several factors (see Wang, 2016; and cited references therein). An effect combined from temperature and fluids in a fault zone can result in thermal pressurization (abbreviated as TP below) which would yield a shear stress (resistance) on the fault plane (Sibson, 1973; Lachenbruch, 1980; Rice, 2006; Wang, 2009, 2011, 2016, 2017a,b,c; Bizzarri, 2009). Rice (2006) proposed two end-member models of TP, i.e., the adiabatic-undrained-deformation (AUD) model and slip-on-a-plane (SOP) model. Since the characteristic distance of the SOP model cannot be associated with the wear process, the SOP model is not used in this study. The AUD model is related to a homogeneous simple strain ε at a constant normal stress σ_n on a spatial scale of the sheared layer. Its shear stress-slip function, $\tau(u)$, is: $\tau(u)=\mu_f(\sigma_n-p_o)exp(-u/u_c)$ (Rice, 2006), which decreases exponentially with increasing u. The characteristic displacement is $u_c=\rho_f C_v h/\mu_f \Lambda$, where ρ_f, C_v, h, μ_f, and Λ are, respectively, the fluid density, heat capacity (in J/°C/kg), the thickness, frictional strength, and the undrained pressurization factor of the fault zone. The parameter Λ is $(\lambda_f-\lambda_n)/(\beta_f+\beta_n)$ where β_f=isothermal compressibility of the pore fluid, β_n=isothermal compressibility of the pore space, λ_f=isobaric, volumetric thermal expansion coefficient for the pore fluid, and λ_n=isobaric, volumetric thermal expansion coefficient for the pore space.

Based on the AUD model, Wang (2009, 2016, 2017a,b,c) took a simplified slip-weakening friction law (denoted by the TP law hereafter):

$$F(u)=F_o exp(-u/u_c). \qquad (2)$$

The value of $F(u)$ at u=0 is F_o, i.e., the static friction force. An example of the plot of $F(u)$ versus u for five values of u_c, i.e., 0.1, 0.3, 0.5, 0.7, and 0.9 m when F_o=1 N/m^2, which are taken from Wang (2016), is displayed in Fig. 3. $F(u)$ decreases with increasing u and its decreasing rate, γ, decreases with increasing u_c. The force drop is lower for larger u_c than for smaller u_c for the same final slip. When $u<<u_c$, $exp(-u/u_c)\approx 1-u/u_c$, thus indicating that u_c^{-1} is almost γ at small u. This TP law is used in this study.

A detailed description about viscosity and the viscous force $\Phi(v)$ can be found in Wang (2016), and only a brief explanation is given below. Jeffreys (1942) first and then numerous authors (Byerlee, 1968; Turcotte and Schubert, 1982; Scholz, 1990; Rice et al., 2001; Wang, 2016) emphasized the viscous effect on faulting due to frictional melts. The viscosity coefficient, υ, of rocks is influenced by T (see Turcotte and Schubert, 1982; Wang, 2011). Spray (2005; and cited references therein) observed a decrease in υ with increasing T. He also stressed that frictional melts with low υ could produce a large volume of melting, thus reducing the effective normal stress. This behaves like fault lubricants during seismic slip.

The physical models of viscosity can be found in several articles (e.g., Cohen, 1979; Hudson, 1980). The stress–strain relationship is $\sigma=E\varepsilon$ where σ and E are, respectively, the stress and the elastic modulus for an elastic body and $\sigma=\upsilon(d\varepsilon/dt)$, where υ is the viscosity coefficient, for a viscous body. Two simple models with a viscous damper and an elastic spring are often used to describe the viscous materials. A viscous damper and an elastic spring are connected in series leading to the Maxwell model and in parallel resulting in the Kelvin-Voigt model (or the Voigt model). According to Hudson (1980), Wang (2016) proposed that the latter is more suitable than the former for seismological problems and thus the Kelvin-Voigt model, whose constitution law is $\sigma(t)=E\varepsilon(t)+\upsilon d\varepsilon(t)/dt$, is taken here and displayed in Fig. 2. The viscous stress is υv.

In order to investigate the viscous effect in a dynamical system, Wang (2016) defined the damping coefficient, η, based on the phenomenon that an oscillating body damps in viscous fluids. According to Stokes' law, $\eta=6\pi R\upsilon$ for a sphere of radius R in a viscous fluid of υ (see Kittel et al., 1968). Hence, the viscous force in Equation 1 is represented by $\Phi=\eta v$. Note that the unit of η is N(m/s)$^{-1}$. Since υ decreases with increasing T, η decreases with increasing T. Hence, η can vary with time during faulting. This point has been studied by Wang (2017b) for the generation of nuclear phase before an earthquake ruptures. In this study, constant η is considered for each case.

Some authors (Knopoff et al., 1973; Cohen, 1979; Rice, 1993; Xu and Knopoff, 1994; Knopoff and Ni, 2001; Bizzarri, 2012a; Dragoni and Santini, 2015) considered that viscosity plays a role on causing seismic radiation to release strain energy during faulting.

3 Normalization of Equation of Motion

Putting Eq. 2 and $\Phi=\eta v$ into Eq. 1 leads to

$$md^2u/dt^2=-K(u-v_pt)-F_o exp(-u/u_c)-\eta v. \qquad (3)$$

Eq. 3 is normalized for easy numerical computations based on the normalization parameters, which is dimensionless: $D_o=F_o/K$, $\omega_o=(K/m)^{1/2}$, $\tau=\omega_o t$, $U=u/D_o$, and $U_c=u_c/D_o$. The normalized velocity, acceleration, and driving velocity are $V=dU/d\tau=[F_o/(mK)^{1/2}]^{-1}du/dt$, $A=d^2U/d\tau^2=(F_o/m)^{-1}d^2u/dt^2$, and $V_p=v_p/(D_o\omega_o)$, respectively. Define $\Omega=\omega/\omega_o$ to be the dimensionless angular frequency, and thus the phase ωt becomes $\Omega\tau$. For the purpose of simplification, $\eta/(mK)^{1/2}$ is denoted by η below. Substituting all normalization parameters into Eq. 3 leads to

$$d^2U/d\tau^2=-U-\eta dU/d\tau-exp(-U/U_c)+V_p\tau. \qquad (4)$$

In order to numerically solve Eq. (4), we define two new parameters, i.e., $y_1=U$ and $y_2=dU/d\tau$. Eq. 4 can be re-written as two first-order differential equations:

$$dy_1/d\tau=y_2 \qquad (5a)$$

$$dy_2/d\tau=-y_1-\eta y_2-exp(-y_1/U_c)+V_p\tau. \qquad (5b)$$

We can numerically solve Eq. 5 by using the fourth-order Runge-Kutta method (Press et al., 1986). In general, the values of D_o are several meters and ω_o are in the range of 0.1 Hz to few Hz (see Wang, 2016). This leads to that $D_o\omega_o$ has an order of magnitude of 1 m/s. The value of V_p must be much smaller than 1 because of $v_p\approx10^{-10}$ m/s. Since the value of V_p mainly influences the recurrence time, T_R, between two events and can only make a very small influence on the pattern of time variations in velocities and displacements of events. In order to study long-term earthquake recurrence, there must be numerous modeled events with clear and visualized time functions of displacements and velocities for an event in the computational time period. If V_p=10^{-10} is considered, T_R is very long and thus τ_D is much shorter than T_R. This makes the time function of an event displayed in the long-term temporal variation in slip looks like just a step function for the displacements and an impulse for the velocities. Hence, in order to get fine visualization a larger value of V_p is necessary. The value of $V_p\tau$ is usually very small during an event and cannot influence the rupture because of a very tiny value of V_p. Numerical test shows that when V_p>10^{-2}, the value of $V_p\tau$ is no t small during an event and can influence the rupture. Hence, V_p=10^{-2} is taken in this study. The backward slip is not allowed in the simulations, because of common behavior of forward earthquake ruptures.

A phase portrait, which is a plot of a physical quantity, *y*, versus another, *x*, i.e., $y=f(x)$, is commonly used to represent nonlinear behavior of a dynamical system (Thompson and Stewart, 1986). The intersection point between $f(x)$ and the bisection line of $y=x$, is defined as the fixed point, that is, $f(x)=x$. If $f(x)$ is continuously differentiable in an open domain near a fixed point x_f and $|f'(x_f)|<1$, attraction can appear at the fixed point. Chaos can also be generated at some attractors. The details can be seen in Thompson and Stewart (1986). In this study, the phase portrait is the plot of V/V_{max} versus U/U_{max}.

4 Simulation Results

Numerical simulations lead to the temporal variations in particle velocities and displacements as displayed in Fig. 1. The values of V_m and D, respectively, represent the peak value of velocity and final slip for each event. Since four cases related to our values of a particular model parameter, there are four values of V_m and D in a figure.

In order to plot the temporal variations in both normalized displacements and velocities, the maximum values of V_m and D of the modelled events, i.e., V_{max} and U_{max}, respectively, are taken into account. The values of V_m and D usually appear in the panel marked by "a" of a figure. Simulation results are shown in Figs. 4–12. The temporal variations in V/V_{max} (displayed by thin solid lines) and cumulative slip $\Sigma U/U_{max}$ (displayed by solid lines) are displayed in the left-handed-side panels. The normalization scales to plot the temporal variations in slip and velocity are V_{max} for the velocities and the final value of $\Sigma U/U_{max}$ for the displacements in the computational time. Hence, the upper bound scale is "1" for the two temporal variations. Hence, only the patterns of temporal variations of velocity and cumulative slip are concerned in these figures.

Simulation results displayed in these figures show that the maximum values of both V and U decrease from case (a) to case (d) in each figure. Hence, the maximum velocity and maximum displacement, which are denoted by V_{max} and U_{max}, respectively, for case (a) can be taken as the scaled factor to normalize the waveforms from case (a) to case (d). This makes us easily to compare the waveforms of the four cases in each figure.

The cases excluding the viscous effect, i.e., η=0, are first simulated and results are shown in Fig. 4 for four values of U_c: (a) for U_c=0.2; (b) for U_c=0.4; (c) for U_c=0.8; and (d) for U_c=1.0. The results of the cases including viscosity, i.e., $\eta \neq 0$, are displayed in Figs. 5–7 for four values of η: (a) for η=0.20; (b) for η=0.40; (c) for η=0.6; and (d) for η=0.8. The values of U_c are 0.2 in Fig. 5, 0.5 in Fig. 6, and 0.8 in Fig. 7.

The left-handed-side panels in Fig. 4 with η=0 show that the peak velocity of an event, V_m, and final slip, D, with the respective maximum values in case (a) as mentioned above, for all simulated events decrease with increasing U_c. From Fig. 3, the force drop, ΔF, decreases with increasing U_c for a certain final slip, thus indicating that larger ΔF yields higher V_m and larger D. This interprets the negative dependence of V_m and D on U_c. When the viscous effect is absent, i.e., η=0, the value of τ_D increases with U_c; while T_R decreases with increasing U_c. When U_c=1, V_m and D are both very small and the system behaves like creeping of a fault. In the right-handed-side panels, there are two fixed points for each case: one is called the non-zero fixed point at larger V and larger U and the other the zero fixed point at V=0 and U=0. The slope at a fixed point is defined to be $d(V/V_{max})/d(U/U_{max})=(U_{max}/V_{max})(dV/dU)$. The absolute values of slope at the two fixed points decrease with increasing U_c, thus suggesting that the fixed point is not an attractor for small U_c and could be an attractor for larger U_c. The phase portrait for U_c=1 is very tiny, because the final slip for U_c=1.0 is much smaller than those for U_c=0.2, 0.4, and 0.8. Hence, U_c=1 will not be taken into account in the following simulations.

The left-handed-side panels in Figs. 5–7 show that V_m and D decrease when either U_c or η increases; while τ_D increases with η and U_c. Meanwhile, T_R increases when either η increases or U_c decreases. The right-handed-side panel exhibits that the phase portraits are coincided for all simulated events for a certain η. The absolute values of slope at the two fixed points decrease when either U_c or η increases. This suggests that the fixed point is not an attractor for small U_c and low η, and can be an attractor for large U_c and high η. Like Fig. 4, the final slip decreases with increasing U_c.

From Figs. 5–7, we can see that the temporal variation in cumulative slip can be described by the perfectly periodic model as mentioned above. Hence, when U_c and η do not change with time, the rate of cumulative slip retains a constant in the computational time period. This is similar to the simulation results with the periodical earthquake occurrences obtained by some authors (e.g., Rice and Tse, 1986; Ryabov and Ito, 2001; Erickson et al., 2008; Mitsui and Hirahara, 2009) based on the one-body model with rate- and state-dependent friction or velocity- weakening friction. But, the present result is inconsistent with the simulation results, from which either the time-predictable model or the slip-predictable model cannot interpret the temporal variation in cumulative slip, based on the same model obtained by others (e.g., He et al., 2003; Bazzarri 2012b; Bizzarri and Crupi, 2014; Kostić et al., 2013a,b; Franović et al., 2016). The differences between the two groups of researchers might be due to distinct additional constrains in respective studies. Although the detailed discussion of such differences is important and significant, it is out of the scope of this study and ignored here.

The phase portraits in Figs. 5–7 exhibit two kinds of fixed points as mentioned above. The absolute values of slope at the non-zero fixed point are higher than 1 and decreases with increasing η. This means that larger η is easier to generate an attractor than small η. However, the reducing rate of absolute value of slope decreases with increasing U_c. The absolute values of slope of the zero fixed point are higher than 1 and decrease with increasing η. This suggests that the zero fixed points can be an attractor. This behavior becomes weaker when U_c increases.

Figs. 4–7 show that when U_c and η are constants during the computational time periods, the general patterns of temporal variations in cumulated slip do not change. Some of the previous studies (e.g., Bizzarri, 2012a,b; and Franović et al., 2016) suggest that the patterns of temporal variations in cumulated slip can change with time. The changes of U_c and η with time should play the main roles. From $u_c=\rho_f C_V h/\mu_f \Lambda$ of the TP model (see Rice 2006), the width of the slipping zone, h, where the maximum deformation is concentrated (Bizzarri, 2009), is a significant parameter in this study. From geological surveys, Rathbun and Marone (2010) observed that *h* is not spatially uniform even within a single fault. Hull (1988) and Marrett and Allmendinger (1990) found that the wear processes occurring during faulting could widen *h*, and thus *h* could vary with time. According to the results gained by several authors (e.g., Power et al., 1988; Robertson, 1983; and Bizzarri, 2010), Bizzarri (2012b) proposed a linear dependence of *h* on the cumulated slip, $S(t)=\sum D(t)$, i.e., $h(t)=CS(t)$ where *C* is a dimensionless increasing rate of *h* with *S* and is considered to be a constant in each case. Based on $h(t)=CS(t)$, the more mature the fault is, the thicker its slip zone is. Since u_c is proportional to *h* and $U_c=u_c/D_o$, U_c is related to *C*. Here, we assume that U_c varies with cumulative slip in the following way: $U_c=U_{co}+C\sum U(t)$ where U_{co} is the initial value of U_c. Simulation results for four values of *C* are shown in Figs. 8–12: (a) for *C*=0.0001; (b) for *C*=0.001; (c) for *C*=0.01; and (d) for *C*=0.05 when η=0 in Figs. 8–10; (a) for *C*=0.0001; (b) for *C*=0.001; (c) for *C*=0.01; and (d) for *C*=0.038 when η=1 in Fig. 11; and (a) for *C*=0.0001; (b) for *C*=0.001; (c) for *C*=0.01; and (d) for *C*=0.0136 when η=1 in Fig. 12. The initial values of U_c are: 0.1 for Fig. 8, 0.5 for Fig. 9, 0.9 for Fig. 10, 0.1 for Fig. 11, and 0.5 for Fig. 12. Note that the value U_c varies with time due to time-varying *h*.

The left-handed-side panels of Figs. 8–12 show that V_m, *D*, τ_D, and T_R are all similar when $C\leq0.001$. However, in general V_m and *D* decrease with increasing *C*; T_R slightly decreases with increasing *C*; and τ_D slightly increases with *C*. A decrease in *D* is particularly remarkable when $C\geq0.01$. When *h* is wider than a critical value with C=0.05 for η=0, normal earthquakes cannot occur and only creeping may happen. The critical value of *h* decreases when the viscous effect is present with η=1 in this study. This decrease is also influenced by U_c: *C*=0.038 when the initial value of U_c is

0.1 and C=0.0136 when the initial value of U_c is 0.5. Obviously, T_R decreases with increasing C, thus leading to a decrease in T_R with increasing h. This is similar to the result obtained by Bizzarri (2010; 2012b). But, the viscous effect was not included in his studies.

The right-handed-side panels of Figs. 8–12 exhibit that the phase portraits for C=0.001 are slightly different from those for C=0.0001 even though the patterns of their variations in V and U are similar; while the phase portraits for C>0.001 are different from those for C≤0.001. An increase in h due to an increase in C with cumulative slip enlarges U_c. This can be explained from Fig. 3 which shows that larger U_c yields a lower ΔF than smaller U_c for the same final slip. Hence, an increase in U_c produces a decrease in ΔF, thus resulting in low V_m and small D. In addition, An increase in U_c makes $exp(-U/U_c)$ approach unity, especially for small U, thus reducing the nonlinear effect caused by TP friction.

Unlike Figs. 4–7, the size of phase portraits in the right-handed-side panels of Figs. 8–12 decreases with increasing C. This reflects a decrease in both T_R and D of events with increasing C as mentioned previously. The absolute values of slope at the non-zero fixed point are higher than 1 and only slightly decrease with time when C<0.01; while the values remarkably decrease with time when C≥0.01. The absolute values of slope at the zero fixed point are higher than 1 and only slightly decrease with time when C<0.01; while those decrease with time when C≥0.01. Results suggest that the non-zero fixed points for all cases in study are not an attractor; and those at the zero fixed points can evolve to an attractor with time when C≥0.01. The phenomenon is particularly remarkable for C=0.05 in Figs. 8–10, C=0.0380 in Fig. 11, and C=0.0136 in Fig. 12, and the evolution is faster for large U_c than for small U_c.

5 Discussion

The simulation results as mentioned previously demonstrate that when U_c and η are constants during the computational time periods, the general patterns of temporal variations in cumulated slip cannot change. In order to investigate the effect of time-vrying η and U_c on the patterns of temporal variations in cumulated slip, we must consider changes of U_c and η with time. The viscosity coefficient can actually vary immediately before and after the occurrence of an earthquake (see Spray, 1883, 2005; Wang, 2017b,c). But, a lack of long-term variation in η does not allow us to explore its possible effect on the change of general patterns of temporal variations in cumulated slip. Here, only the possible effect due to time-varying U_c.

As mentioned above, the equality $U_c=u_c/D_o$ leads to $U_c=\rho_f C_V h/\mu_f D_o \Lambda$. Obviously, U_c is controlled by six factors, i.e., ρ_f, C_V, h, μ_f, D_o, and Λ. Since the tectonics of a region is generally stable during a long time, the value of $D_o=F_o/K$ could not change too much and thus would not influence U_c. The Debye law (cf. Reif, 1965) gives $C_v \sim (T+273.16)^3$, where 273.16 is the value to convert temperature from Celsius to Kelvin, at low T and $C_v \approx$constant at high T. The threshold temperature, from which C_v begins to approach a constant, is 200−300 ^{o}K. In this study, C_v is almost a constant because of T>250 ^{o}C=523.16 ^{o}K, which is the average ambient temperature of fault zone with depths ranging from 0 to 20 km. Hence, C_v is almost constant during a long time and thus cannot influence U_c.

The frictional strength, μ_f, is influenced by several factors including humidity, temperature, sliding velocity, strain rate, normal stress, thermally activated rheology etc (Marone, 1998; Rice, 2006), and thus can change with time (Sibson, 1992; Rice, 2006). Hirose and Bystricky (2007) observed that serpentine dehydration and subsequent fluid pressurization due to co-seismic frictional heating may reduce μ_f and thus promote further weakening in a fault zone. The pore fluid pressure exists in wet rocks, yet not in dry rocks. Clearly, the time variation in μ_f can affects the earthquake recurrences. However, a lack of long-term observations of μ_f during a seismic cycle makes the studies of its effect on earthquake recurrence be impossible.

The fluid density ρ_f and the porosity n depend on T and p. Although there are numerous studies on such dependence (Lachenbruch, 1980; Bizzarri, 2012b; and cited references therein), observed data and theoretical analyses about the values of ρ_f and n during a seismic cycle are rare.

The porosity is associated with the permeability, κ. Bizzarri (2012c) pointed out that the time-varying permeability, $\kappa(t)$, and porosity of a fault zone (cf. Mitsui and Cocco, 2010; Bizzarri, 2012b) can reduce T_R. One of the Kozeny–Carman's (KC) relations (Costa, 2006; and references cited therein) is: $\kappa(t)=\kappa_C\phi^2(t)d^3(t)/[1-\phi(t)]^2$, where κ_C is a dimensionless constant depending on the material in consideration; ϕ is V_{voids}/V_{tot} where V_{voids} and V_{tot} are, respectively, the pore volume and the total volume of the porous materials; and d is the (average) diameter of the grains, ranging between 4×10^{-5} m and 1×10^{-4} m (Niemeijer et al., 2010). Usually, κ, ϕ, and d can vary in the fault zone (Segall and Rice, 1995). After faulting κ and ϕ would change and d becomes smaller because of refining of the grains. According to this relation, Bizzarri (2012b) found that $\kappa(t)$ could significantly reduce T_R in comparison with the base model with constant κ. The reason is explained below. An increase in permeability can result in an increase in pore pressure, p_f. This can reduce the frictional resistance from $\tau=\mu(\sigma_n-p_f)$ and thus could trigger earthquakes earlier. Hence, the time-varying permeability can change T_R. Nevertheless, we cannot investigate its influence on earthquake recurrence here because there is a lack of a long-term observation of hydraulic parameters during a seismic cycle.

It is significant to explore the factors that can yield a non-perfectly periodic seismic cycle. The width of the slipping zone, *h*, can be a candidate as pointed out by some authors (e.g., Bizzarri, 2009; Rathbun and Marone, 2010). Since the displacement along a fault is controlled by the fault rheology, *h* should depend on the rheology on the sliding interface. The wear processes occurring during faulting could widen *h* (Hull, 1988; Marrett and Allmendinger, 1990). According to the results gained by several authors (e.g., Power et al., 1988; Robertson, 1983; and Bizzarri, 2010), Simulation results for various values of *C* and the results are shown in Figs. 8–10 with η=0 and in Figs. 11–12 with η=1. Results exhibit that when *C*>0.0001, the wear process affects the recurrence of slip and the effect increases with *C* and when *C* is larger than an upper-bound value, larger-sized events cannot occur and the earthquake recurrence does not exist. Both T_R and *D* decrease when the fault becomes more mature due to a thicker slip zone. Meanwhile, the viscous effect can also play a secondary role on the earthquake recurrence because it makes upper-bound value become smaller. Although either the time- or slip-predictable model can describe the temporal variations of cumulative slip of events occurring in the earlier time period, they cannot interpret those of events in the later parts. This might suggest that it is more difficult to produce large earthquakes along a fault when it becomes more mature, especially for the cases with viscosity. This implicates that seismic hazard is higher for a young fault than a mature one. Hence, it is significant and important to identify the width of slip zone of an earthquake fault for seismic hazard estimates.

6 Conclusions

To study the frictional and viscous effects on earthquake recurrence, numerical simulations of the temporal variations in cumulative slip have been conducted based on the normalized equation of a one-body model in the presence of thermal-pressurized slip-weakening friction and viscosity. The wear process, which is included in the friction law, is also taken into account. The model parameters of friction and viscosity are represented, respectively, by U_c and η, where $U_c=u_c/D_o$ is the normalized characteristic distance and η is the normalized damping coefficient. Numerical simulation of the time variations in V/V_{max} and cumulative slip $\Sigma U/U_{max}$, and the phase portrait of V/V_{max} versus U/U_{max} are made for various values of U_c and η.

Results exhibit that both friction and viscosity remarkably affect earthquake recurrences. The recurrence time, T_R, increase when η increases or U_c decreases. The final slip, D, and the duration time of slip, τ_D, of an event slightly decrease when η or τ_D increases and slightly increases with U_c. Considering the effect due to wear process, the thickness of slip zone, h that depends on the cumulated slip, $S(t)=\sum D(t)$, i.e., $h(t)=CS(t)$ (C=a dimensionless constant), is an important factor in influencing earthquake recurrences. U_c increases with $\sum U$ with an increasing rate of C. When C>0.0001, the wear process influences the recurrence of slip and the effect increases with C. When C is larger than an upper-bound value, larger-sized events cannot occur and the earthquake recurrence does not exist. If the slip zone becomes thicker, the fault is more mature. This makes T_R and D become shorter. This might suggest that it is more difficult to produce large earthquakes along a fault when it becomes more mature. This phenomenon becomes remarkable when the viscous effect exists because the upper-bound value becomes smaller. The temporal variation in slip cannot be interpreted by the time-predictable or slip-predictable model when the fault is affected by wear process with large C. In addition, the size of phase portrait of V/V_{max} versus

U/U_{max} decreases with increasing *C*. This again reflects decreases in both T_R and *D* of events with increasing *C* as inferred from the temporal variations in cumulative slip.

Acknowledgments The author would like to thank Prof. Filippos Vallianatos (Editor of NHESS) and two anonymous reviewers for their valuable comments and suggestions to help me to substantially improve this article. The study was financially supported by Academia Sinica and the Ministry of Science and Technology (Grant No.: MOST-106-2116-M-001-005).

References

Abaimov, S.G., Turcotte D.L., Shcherbakov R., and Rundle J.B.: Recurrence and interoccurrence behavior of self-organized complex phenomena, Nonlin. Processes Geophys., 14, 455-464, 2007

Abe, Y. and Kato N.: Complex earthquake cycle simulations using a two-degree-of-freedom spring-block model with a rate- and state-friction law, Pure. Appl. Geophys., 170, 745-765, 2013.

Ando, M.; Source mechanisms and tectonic significance of historic earthquakes along the Nankai trough, Japan, Tectonpohys,, 27, 119-140, 1975

Bakun, W.H. and McEvilly T.V.: Earthquakes near Parkfield, California: comparing the 1934 and 1966 sequences, Science, 205, 1375-1377, 1979.

Bakun, W.H. and McEvilly T.V.: Recurrence models and Parkfield, California, earthquakes, J. Geophys. Res., 89, 3051-3058, 1984.

Beeler, N.M., Lockner D.L., and Hickman S.H.: A simple stick-slip model for repeating earthquakes and its implication for microearthquakes at Parkfield, Bull. Seism. Soc. Am., 91(6), 1797-1804, 2001.

Belardinelli, M.E. and Belardinelli E.: The quasi-static approximation of the spring-slider motion. Nonl. Processes Geophys., 3, 143-149, 1996.

Bizzarri, A.: What does control earthquake ruptures and dynamic faulting? A review of different competing mechanism, Pure. Appl. Geophys., 166, 741-776, 2009.

Bizzarri. A.: On the recurrence of earthquakes: Role of wear in brittle faulting, Geophys. Res., Letts., 37, L20315, http://dx.doi.org/10.1029/2010GL045480, 2010.

Bizzarri, A.: Modeling repeated slip failures on faults governed by slip- weakening friction, Bull. Seism. Soc. Am., 102(2), 812-821 doi:10.1785/0120110141, 2012a.

Bizzarri, A.: What can physical source models tell us about the recurrence time of earthquakes?, Earth-Sci. Rev., 115, 304-318 http://dx.doi.org/10.1016/j.earscirev. 2012.10.004, 2012b

Bizzarri., A.: Effects of permeability and porosity evolution on simulated earthquakes, J. Struct. Geol., 38, 243-253, http://dx.doi.org/10.1016/j.jsg.2011.07.009, 2012c

Bizzarri, A. and Crupi P.: Linking the recurrence time of earthquakes to source parameters: A dream or a real possibility?, Pure. Appl. Geophys., 171, 2537-2553, DOI:10.1007/s00024-013-0743-1, 2014.

Brun, J.L. and Gomez A.B.: A four-parameter, two degree-of-freedom block-spring model: Effect of the driver velocity, Pure. Appl. Geophys., 143(4), 633-653, 1994.

Burridge, R. and Knopoff L.: Model and theoretical seismicity, Bull. Seism. Soc. Am., 57, 341-371, 1967.

Byerlee, J.D.: Brittle-ductile transition in rocks, J. Geophys. Res., 73, 4711-4750, 1968.

Carlson, J.M. and Langer J.S: Mechanical model of an earthquake fault, Phys. Rev. A, 40, 6470-6484, 1989.

Chen, K.H., Nadeau R.M., and Rau R.J.: Towards a universal rule on the recurrence interval scaling of repeating earthquakes?, Geophys. Res., Letts., 34, L16308, doi:10.1029/2007GL030554, 2007.

Cohen, S.: Numerical and laboratory simulation of fault motion and earthquake occurrence, Rev. Geophys. Space Phys., 17(1), 61-72, 1979.

Costa, A.: Permeability-porosity relationship: a reexamination of the Kozeny–Carman equation based on a fractal pore-space geometry assumption, Geophys. Res. Letts., 33, L02318 http://dx.doi.org/10.1029/2005GL025134, 2006.

Davis, P.M., Jackson D.D., and Kagan Y.Y.: The longer it has been since the last earthquake, the longer the expected time till the next?, Bull. Seism. Soc. Am., 79:1439-1456, 1989.

Dragoni, M. and Piombo A.: Dynamics of a seismogenic fault subject to variable strain rate, Nonlin. Processes Geophys., 18, 431-439, doi:10.5194/npg-18-431-2011, 2011.

Dragoni, M. and Santini S.: A two-asperity fault model with wave radiation, Phys. Earth Planet. Inter., 248, 83-93, 2015.

Enescu, B., Struzik Z., and Kiyono K.: On the recurrence time of earthquakes: insight from Vrancea (Romania) intermediate-depth events, Geophys. J. Int., 172, 395-404, doi:10.1111/j.1365-246X.2007.03664.x, 2008.

Erickson, B., Birnir1 B., and Lavall´ee D.: A model for aperiodicity in earthquakes, Nonlin. Processes Geophys., 15, 1-12, 2008.

Erickson, B., Birnir B., and Lavall´ee D.: Periodicity, chaos and localization in a Burridge–Knopoff model of an earthquake with rate-and-state friction, Geophys. J. Int., 187, 178-198, doi:10.1111/j.1365-246X.2011.05123.x, 2011.

Franovic´, I., Kostic´ S., Perc M., Klinshov V., Nekorkin V., and Kurths J.: Phase response curves for models of earthquake fault dynamics, Chaos, 26, 063105, http://dx.doi.org/10.1063/1.4953471, 2016.

Hasumi, T.: Interoccurrence time statistics in the two-dimensional Burridge- Knopoff earthquake model, Phys. Rev. E, 76, 026117, DOI:10.1103/PhysRevE.76.026117, 2007.

He, C., Wong T.f., and Beeler N.M.: Scaling of stress drop with recurrence interval and loading velocity for laboratory-derived fault strength relations, J. Geophys. Res., 108(B1), 2037 doi:10.1029/2002JB001890, 2003.

Hirose, T. and Bystricky M.: Extreme dynamic weakening of faults during dehydration by coseismic shear heating, Geophys. Res., Letts., 34, L14311 doi:10.1029/2007GL030049, 2007.

Huang, J. and Turcotte D.L.: Are earthquakes an example of deterministic chaos?, Geophys. Res., Letts., 17(3), 223-226, 1990.

Huang, J. and Turcotte D.L.: Evidence of chaotic fault interactions in the seismicity of the San Andreas fault and Nankai trough, Nature, 348, 234-236, 1992.

Hudson, J.A.: The excitation and propagation of elastic waves. Cambridge Monographs on Mechanics and Applied Mathematics, Cambridge Univ. Press, 226 pp., 1980.

Hull, J.: Thickness–displacement relationships for deformation zones, J. Struct. Geol., 10, 431-435, http://dx.doi.org/10.1016/0191-8141(88)90020-X, 1988.

Jeffreys, H.: On the mechanics of faulting, Geol. Mag., 79, 291, 1942.

Kanamori, H. and Allen C.R.: Earthquake repeating time and average drop, In: Das et al. (eds.) Earthquake Source Mechanics Maurice Ewing Series 6, AGU, 227-235, 1986.

Kittel C, Knight WD, Ruderman MA (1968) Mechanics. Berkeley Physics Course vol 1 McGraw-Hill Book Co New York, 1986.

Knopoff, L., and Ni X.X.: Numerical instability at the edge of a dynamic fracture, Geophys. J. Int., 147, F1-F6, 2001.

Knopoff, L., Mouton J.Q., and Burridge R.: The dynamics of a one-dimensional fault in the presence of friction, Geophys. J. R. astro. Soc., 35, 169-184, 1973.

Kostić, S., Franović I., Todorović K., and Vasoví N.: Friction memory effect in complex dynamics of earthquake model, Nonlin. Dyn. 73, 1933-1943, DOI:10. 1007/s11071-013-0914-8, 2013a.

Kostić, S., Vasoví N., Franović I., and Todorović K.: Dynamics of simple earthquake model with time delay and variation of friction strength, Nonlin. Processes Geophys., 20, 857-865, doi:10.5194/npg-20-857-2013, 2013b.

Lachenbruch, A.H.: Frictional heating, fluid pressure, and the resistance to fault motion, J. Geophys. Res., 85, 6097-6122, 1980.

Lapusta, N. and Rice J.R.: Nucleation and early seismic propagation of small and large events in a crustal earthquake model, J. Geophys. Res., 108, 1-18, 2003.

Marone, C.: Laboratory-derived friction laws and their application to seismic faulting, Ann. Rev. Earth Planet. Sci., 26, 643-669, 1998.

Marrett, R. and Allmendinger R.W.: Kinematic analysis of fault-slip data, J. Struct. Geol., 12, 973-986, doi.org/10.1016/0191-8141(90)90093-E, 1990.

Mitsui, Y. and Cocco M.: The role of porosity evolution and fluid flow in frictional instabilities: a parametric study using a spring-slider dynamic system, Geophys. Res., Letts., 37, L23305, doi.org/10.1029/2010GL045672, 2010.

Mitsui, Y. and Hirahara K.: Coseismic thermal pressurization can notably prolong earthquake recurrence intervals on weak rate and state friction faults: numerical experiments using different constitutive equations, J. Geophys. Res., 114, B09304, doi.org/10.1029/2008JB006220, 2009.

Murray, J. and Segall P.: Testing time-predictable earthquake recurrence by direct measurement of strain accumulation and release, Nature, 49, 287-291, 2002.

Nadeau, R.M. and Johnson L.R.: Seismological studies at Parkfield VI moment release rates and estimates of source parameters for small repeating earthquake, Bull. Seism. Soc. Am., 88, 790-814, 1998.

Niemeijer, A., Marone C., and Ellsworth D.: Frictional strength and strain weakening in simulated fault gouge: competition between geometrical weakening and chemical strengthening, J. Geophys. Res., 115, B10207, doi.org/10.1029/2009JB000838, 2010.

Nur, A.: Nonuniform friction as a physical basis for earthquake mechanics, Pure. Appl. Geophys., 116, 964-989, 1978.

Okada, T., Matsuzawa T., and Hasegawa A.: Comparison of source areas of M4.8+/-0.1 repeating earthquakes off Kamaishi, NE Japan: are asperities persistent features?, Earth Planet. Sci. Letts., 213(3-4), 361-374, doi.org/10.1016/S0012-821X(03000299-1, 2003.

Power, W.L., Tullis T.E., and Weeks D.J.: Roughness and wear during brittle faulting, J. Geophys. Res., 93, B12, 15268-15278, doi.org/10.1029/JB093iB12p15268, 1988.

Press, WH.., Flannery B.P., Teukolsky S.A., and Vetterling W.T.: Numerical Recipes, Cambridge Univ. Press Cambridge, 1986.

Rathbun, A.P. And Marone C.: Effect of strain localization on frictional behavior of sheared granular materials, J. Geophys. Res., 115, B01204 doi.org/10.1029/2009JB006466, 2010.

Reid, H.F.: The California earthquake of April 18, 1906, In: Report of the State Investigation Commission 2, Mechanics of the Earthquake Carnegie Inst Washington, D.C., 1910.

Reif, F.: Fundamentals of statistical and thermal physics, McGraw-Hill, New York, 651 pp., 1965.

Rice, J.R.: Spatio-temporal complexity of slip on a fault, J. Geophys. Res., 98, B6, 9885-9907, 1993.

Rice, J.R.: Heating and weakening of faults during earthquake slip, J. Geophys. Res., 111, B05311, doi:10.1029/2005JB004006, 2006.

Rice, J.R. and Tse S.T.: Dynamic motion of a single degree of freedom system following a rate and state dependent friction law, J. Geophys. Res., 91, B1, 521-530, 1986.

Rice, J.R., Lapusta N., and Ranjith K.: Rate and state dependent friction and the stability of sliding between elastically deformable solids, J. Mech. Phys. Solids, 49, 1865-1898, 2001.

Robertson, E.C.: Relationship of fault displacement to gouge and breccia thickness, Mining Engin., 35, 1426-1432, 1983.

Rubinstein, J.L., Ellsworth W.L., Beeler N.M., Kilgore B.D., Lockner D.A., and Savage H.M.: Fixed recurrence and slip models better predict earthquake behavior than the time- and slip-predictable models: 2. Laboratory earthquakes, J. Geophys. Res.,117, B02307, doi:10.1029/2011JB008723, 2012.

Ryabov, V.B. and Ito K.: Intermittent phase transitions in a slider-spring model as a mechanism for earthquakes, Pure. Appl. Geophys., 158:919-930, 2001.

Scholz, C.H.: The Mechanics of Earthquakes and Faulting. Cambridge Univ. Press Cambridge, 439 pp., 1990.

Schwartz, D.P. and Coppersmith K.S.: Fault behavior and characteristic earthquakes: examples from the Wasatch and San Andreas fault zones, J. Geophys. Res., 89, 5681-5698, 1984.

Segall, P. and Rice J.R.: Dilatancy, compaction, and slip instability of a fluid-infiltrated fault, J. Geophys. Res., 100, 22155-22171, 1995.

Shimazaki, K. and Nakata T.: Time-predictable model for large earthquakes, Geophys. Res. Letts., 7, 279-282, doi.org/10.1029/GL007i004p00279, 1980.

Sibson, R.H.: Interaction between temperature and pore-fluid pressure during earthquake faulting and a mechanism for partial or total stress release, Natural Phys. Sci., 243, 66-68, 1973.

Sibson, R.H.: Implications of fault-valve behavior for rupture nucleation and recurrence, Tectonophys., 211,283-293, 1992.

Sieh, K.: A review of geological evidence for recurrence times of large earthquakes, In: Earthquake Prediction−An International Review, Mauric Ewing Series, 4, AGU, 181-207, 1981.

Sieh, K., Natawidjaja D., Meltzner A.J., Shen C.C., and Cheng H.: Earthquake supercycles inferred from sea-level changes recorded in the corals of West Sumatra, Science, 322, 1674-1678, 2008.

Sykes, L.R. and Quittmeyer R.C.: Repeat times of great earthquakes along simple plate boundaries, In: Earthquake Prediction−An International Review, Maurice Ewing Series 4, AGU, 217-247, 1981.

Spray, J.G.: Viscosity determinations of some frictionally generated silicate melts: Implications for fault zone rheology at high strain rates, J. Geophys. Res., 98, B5, 8053-8068, 1983.

Spray, J.G.: Evidence for melt lubrication during large earthquakes, Geophys. Res., Letts., 32, L07301, doi:10.1029/2004GL022293, 2005.

Sykes, L.R. and Menke W.: Repeat times of large earthquakes: implications for earthquake mechanics and long-term prediction, Bull. Seism. Soc. Am., 96(5), 1569-1596, doi.org/10.1785/0120050083, 2006.

Thompson., J.M.T. and Stewart H.B.: Nonlinear Dynamics and Chaos. John Wiley and Sons, New York, 376 pp., 1986.

Turcotte, D.L.: Fractal and Chaos in Geology and Geophysics, Cambridge Univ. Press, New York, 221 pp., 1992.

Turcotte, D.L. and Schubert G.: GEODYNAMICS – Applications of Continuum Physics to Geological Problems, Wiley, 450 pp., 1982

Wang, J.H.: Effect of seismic coupling on the scaling of seismicity, Geophys. J. Int., 121, 475-488, 1995.

Wang, J.H.: Velocity-weakening friction law as a factor in controlling the frequency-magnitude relation of earthquakes, Bull. Seism. Soc. Am., 86, 701-713, 1996.

Wang, J.H.: Instability of a two-dimensional dynamical spring-slider model of an earthquake fault, Geophys. J. Int., 143, 389-394, 2000.

Wang, J.H.: A one-body model of the 1999 Chi-Chi, Taiwan, earthquake, Terr. Atmos. Ocean. Sci., 14(3), 335-342, 2003.

Wang, J.H.: Earthquakes rupturing the Chelungpu fault in Taiwan are time-predictable, Geophys. Res. Lett., 32, L06316 doi:10.1029/2004GL021884, 2005.

Wang, J.H.: A dynamic study of the frictional and viscous effects on earthquake rupture: a case study of the 1999 Chi-Chi earthquake, Taiwan, Bull. Seism. Soc. Am.,97(4), 1233-1244, 2007.

Wang, J.H.: One-dimensional dynamical modeling of earthquakes: A review, Terr.

Atmos. Ocean. Sci., 19, 183-203, 2008.

Wang, J.H.: Effect of thermal pressurization on the radiation efficiency, Bull. Seism. Soc. Am., 99(4), 2293-2304, 2009.

Wang, J.H.: Thermal and pore fluid pressure history on the Chelungpu fault at a depth of 1111 meters during the 1999 Chi-Chi, Taiwan, earthquake, J. Geophys. Res., 116, B03302 doi:10.1029/2010JB007765, 2011.

Wang, J.H.: Some intrinsic properties of the two-dimensional dynamical spring-slider model of earthquake faults, Bull. Seism. Soc. Am., 102(2), 822-835, 2012

Wang, J.H.: Slip of a one-body spring-slider model in the presence of slip-weakening friction and viscosity, Ann. Geophys., 59(5), S0541, DOI:10.4401/ag-7063, 2016.

Wang, J.H.: Slip of a two-degree-of-freedom spring-slider model in the presence of slip-weakening friction and viscosity, Ann. Geophys., 60(6), S0659, doi:10. 4401/ag-7295, 2017a.

Wang, J.H.: Frictional and viscous effects on the nucleation phase of an earthquake nucleation, J. Seismol., 21(6), 1517-1539, 2017b.

Wang, J.H.: Multi-stable slip in a one-degree-of-freedom spring-slider model with thermal-pressurized friction and viscosity, Nonl. Processes Geophys., 24, 467-480, doi.org/10.5194/npg-24-467-2017, 2017c

Wang, J.H. and Hwang R.D.: One-dimensional dynamical simulations of slip complexity of earthquake faults, Earth Planets Space 53, 91-100, 2001.

Wang, J.H. and Kuo C.H.: On the frequency distribution of inter-occurrence times of earthquakes, J. Seismol., 2, 351-358, 1998.

Ward, S.N.: A synthetic seismicity model for southern California: Cycles, probabilities, and hazard, J. Geophys. Res., 101, 22393-22418, 1996.

Ward, S.N.: San Francisco Bay Area earthquake simulations: A step toward a standard physical earthquake model, Bull. Seism. Soc. Am., 90, 370-386, 2000.

Xu, H.J. and Knopoff L.: Periodicity and chaos in a one-dimensional dynamical model of earthquakes, Phys. Rev. E., 50(5), 3577-3581, 1994.

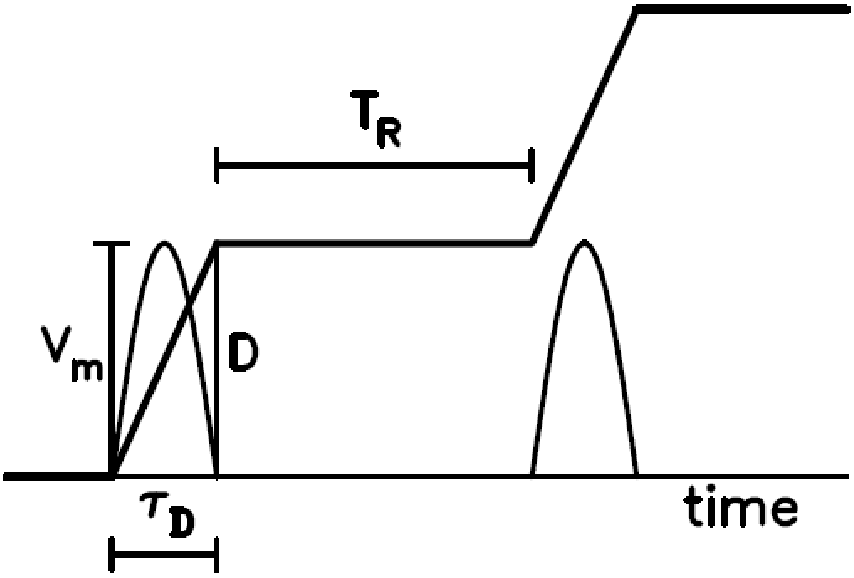

Figure 1. A general pattern of time variations in slip (thick solid line) and particle velocity (thin solid curve) during a seismic cycle: T_R=the recurrence time or the inter-event time of two events in a seismic cycle; τ_D=the duration time of slip of an event; D=the final slip of an event; and V_m=the peak particle velocity of an event.

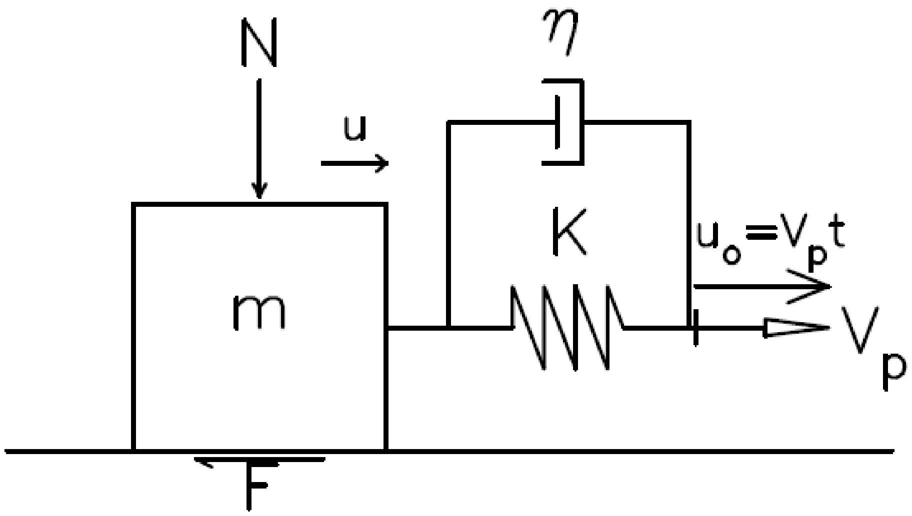

Figure 2. One-body spring-slider model. In the figure, t, m, K, η, V_p, N, F u, and u_o denote, respectively, the time, the mass of the slider, the spring constant, the damping coefficient, the driving velocity, the normal force, the frictional force, displacement of the slider, and the equilibrium location of the slider. (after Wang, 2016)

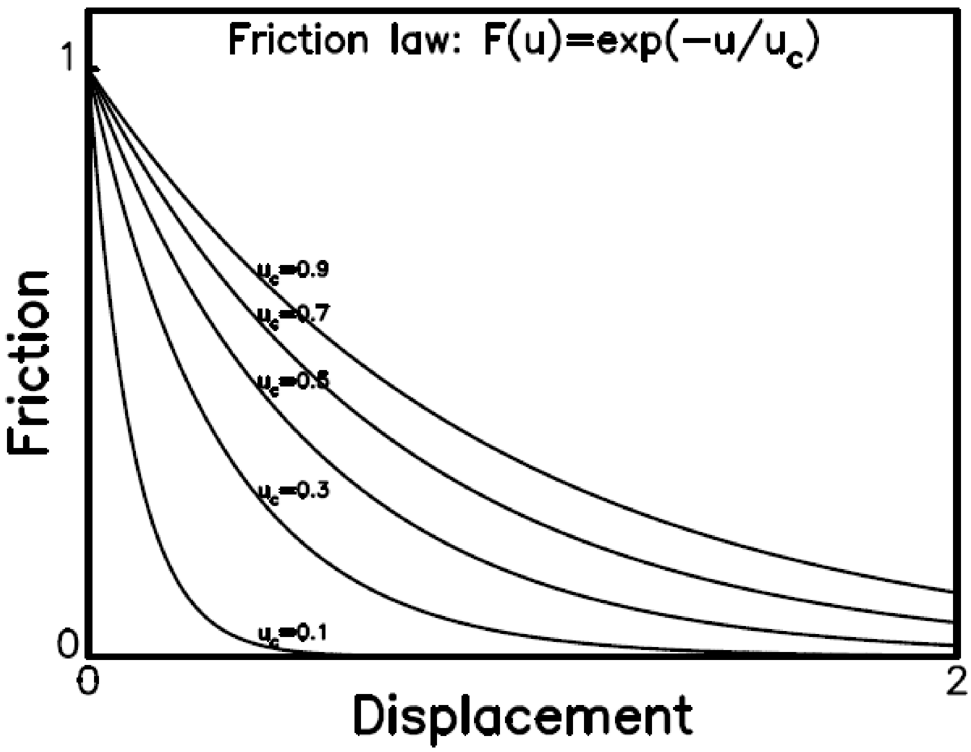

Figure 3. The plots of $F(u)=F_o exp(-u/u_c)$ versus u when u_c=0.1, 0.3, 0.5, 0.7, and 0.9 m when F_o=1 Nt/m^2. (after Wang, 2016)

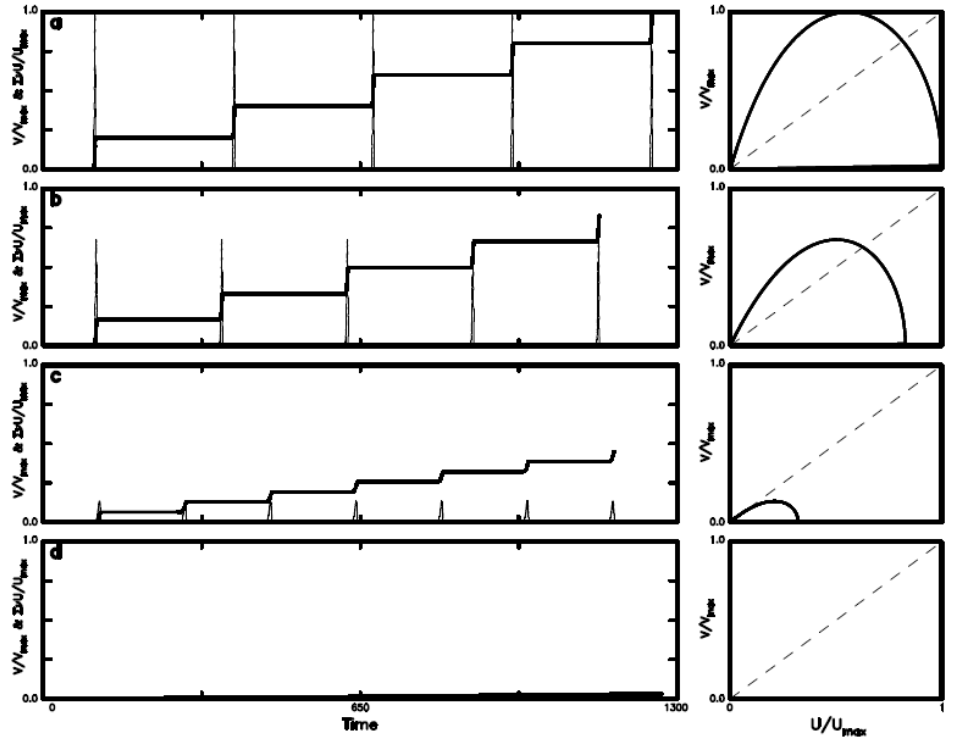

Figure 4. The time variations in V/V_{max} (thin solid line) and cumulative slip $\Sigma U/U_{max}$ (solid line) and the phase portrait of V/V_{max} versus U/U_{max} (solid line) for four values of U_c: (a) for U_c=0.2; (b) for U_c=0.4; (c) for U_c=0.8; and (d) for U_c=1.0 when η=0.0.

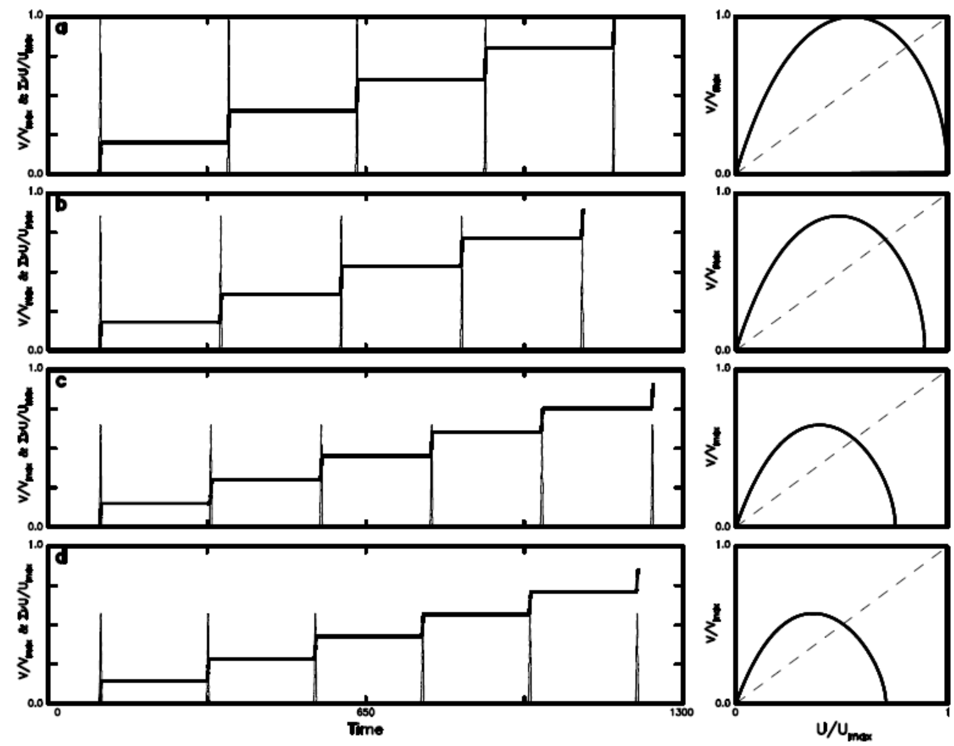

Figure 5. The time variations in V/V_{max} (thin solid line) and cumulative slip $\Sigma U/U_{max}$ (solid line) and the phase portrait of V/V_{max} versus U/U_{max} (solid line) for four values of η: (a) for η=0.2; (b) for η=0.4; (c) for η=0.8; and (d) for η=1.0 when U_c=0.2.

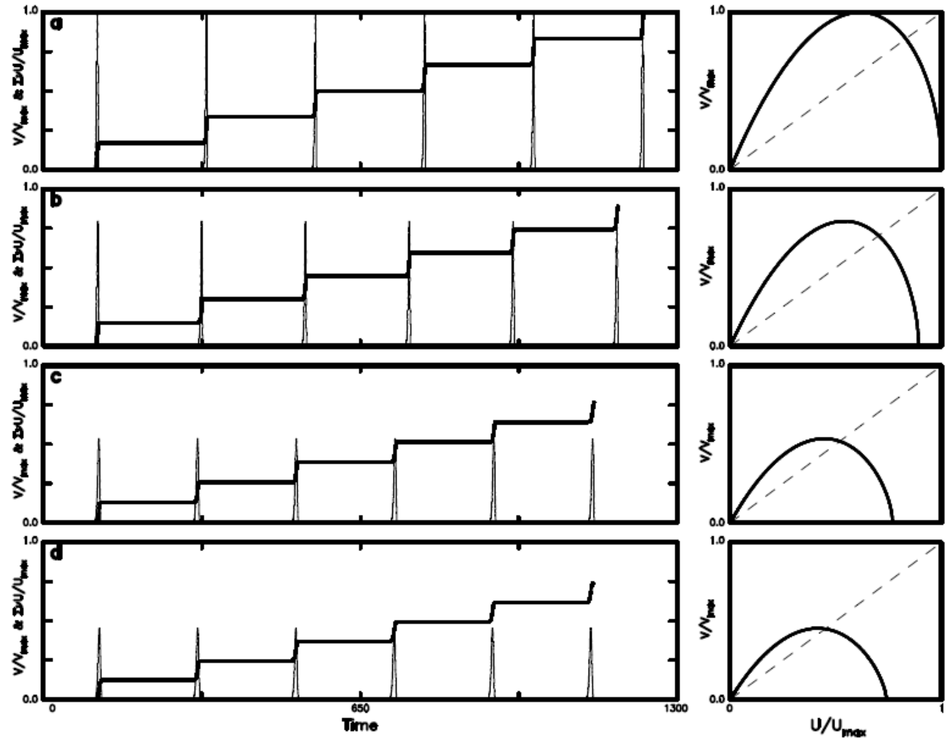

Figure 6. The time variations in V/V_{max} (thin solid line) and cumulative slip $\Sigma U/U_{max}$ (solid line) and the phase portrait of V/V_{max} versus U/U_{max} (solid line) for four values of η: (a) for η=0.2; (b) for η=0.4; (c) for η=0.8; and (d) for η=1.0 when U_c=0.5.

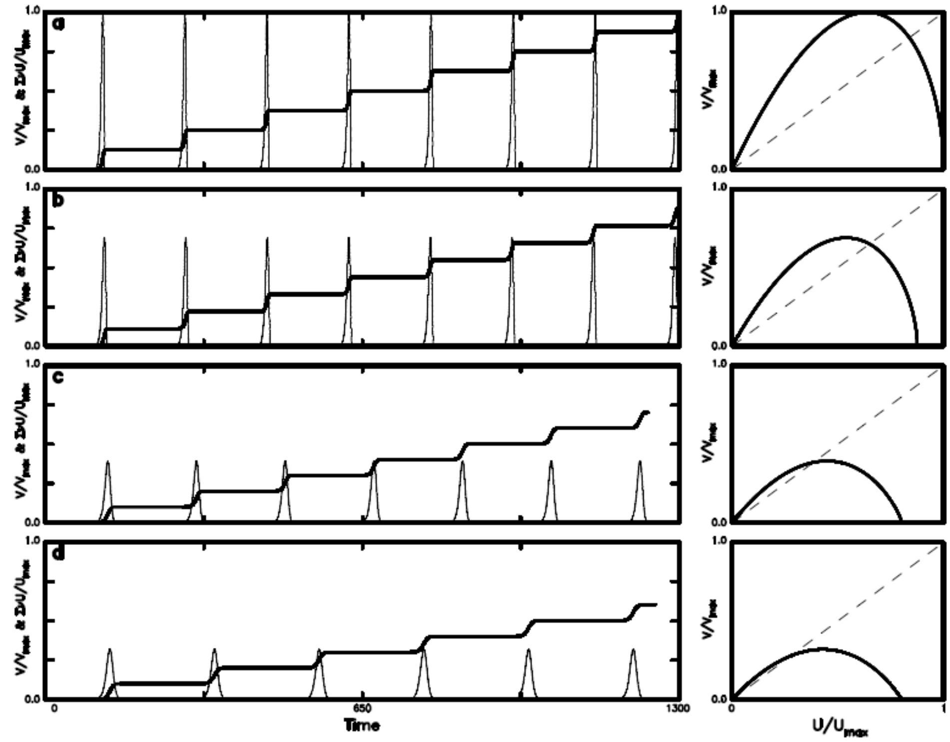

Figure 7. The time variations in V/V_{max} (thin solid line) and cumulative slip $\Sigma U/U_{max}$ (solid line) and the phase portrait of V/V_{max} versus U/U_{max} (solid line) for four values of η: (a) for η=0.2; (b) for η=0.4; (c) for η=0.8; and (d) for η=1.0 when U_c=0.8.

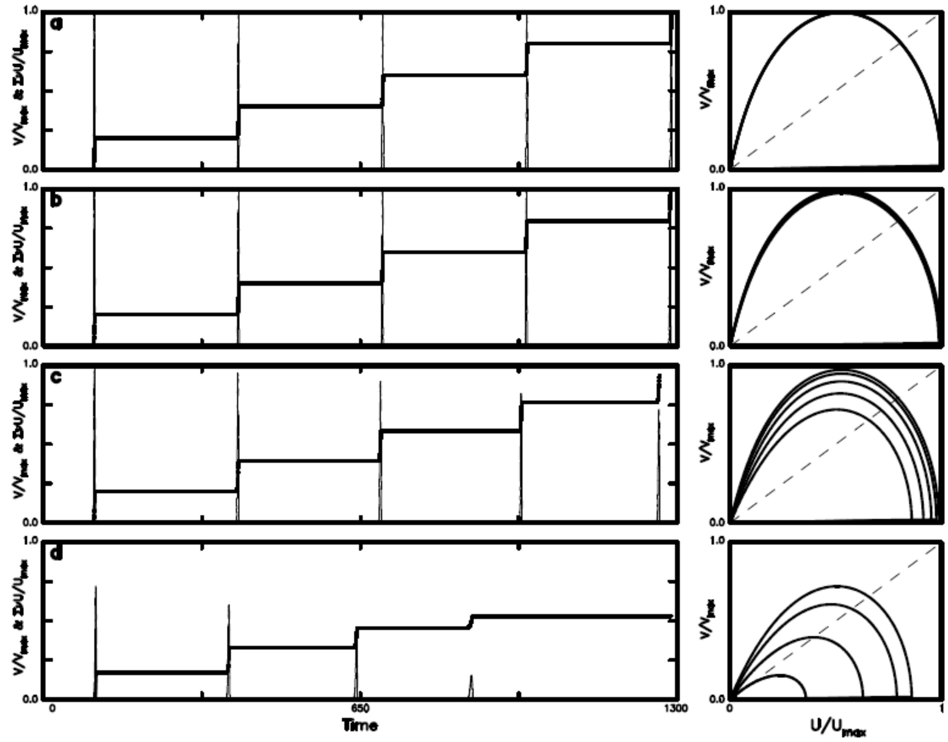

Figure 8. The time variations in V/V_{max} (thin solid line) and cumulative slip $\Sigma U/U_{max}$ (solid line) and the phase portrait of V/V_{max} versus U/U_{max} (solid line) for four values of C: (a) for C=0.0001; (b) for C=0.001; (c) for C=0.01; and (d) for C=0.05 when U_{co}=0.1 and η=0.

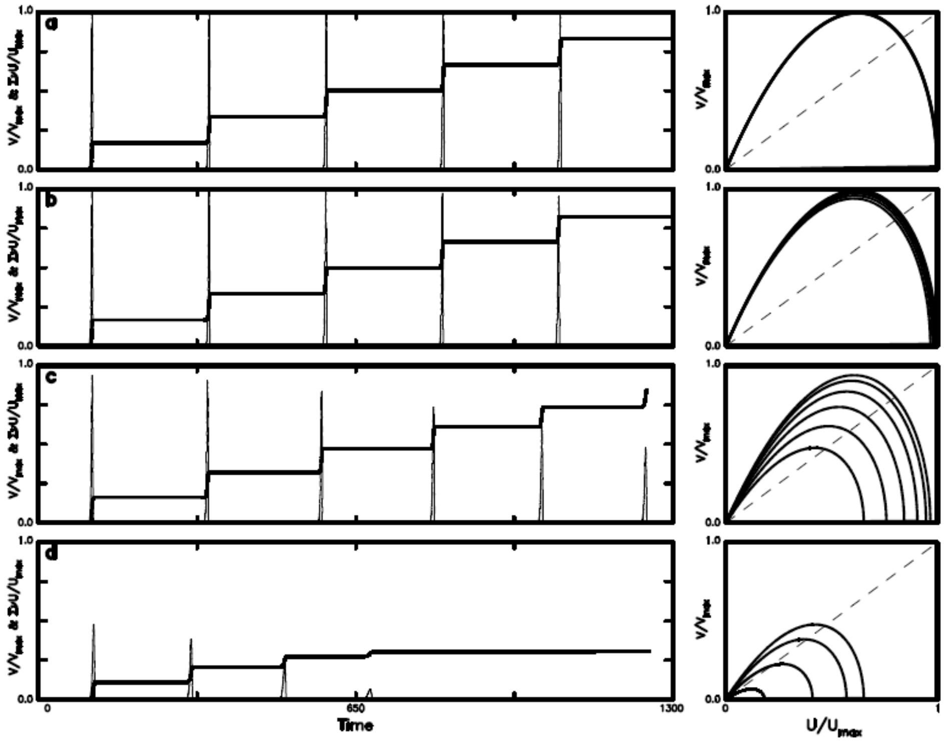

Figure 9. The time variations in V/V_{max} (thin solid line) and cumulative slip $\Sigma U/U_{max}$ (solid line) and the phase portrait of V/V_{max} versus U/U_{max} (solid line) for four values of C: (a) for C=0.0001; (b) for C=0.001; (c) for C=0.01; and (d) for C=0.05 when U_{co}=0.5 and η=0.

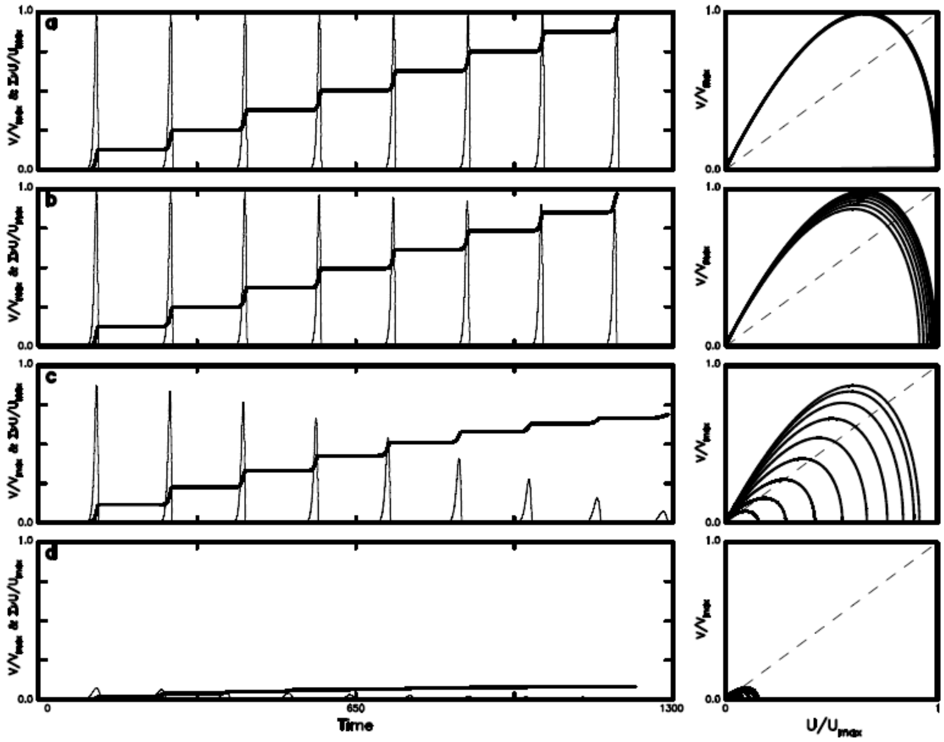

Figure 10. The time variations in V/V_{max} (thin solid line) and cumulative slip $\Sigma U/U_{max}$ (solid line) and the phase portrait of V/V_{max} versus U/U_{max} (solid line) for four values of C: (a) for C=0.0001; (b) for C=0.001; (c) for C=0.01; and (d) for C=0.05 when U_{co}=0.9 and η=0.

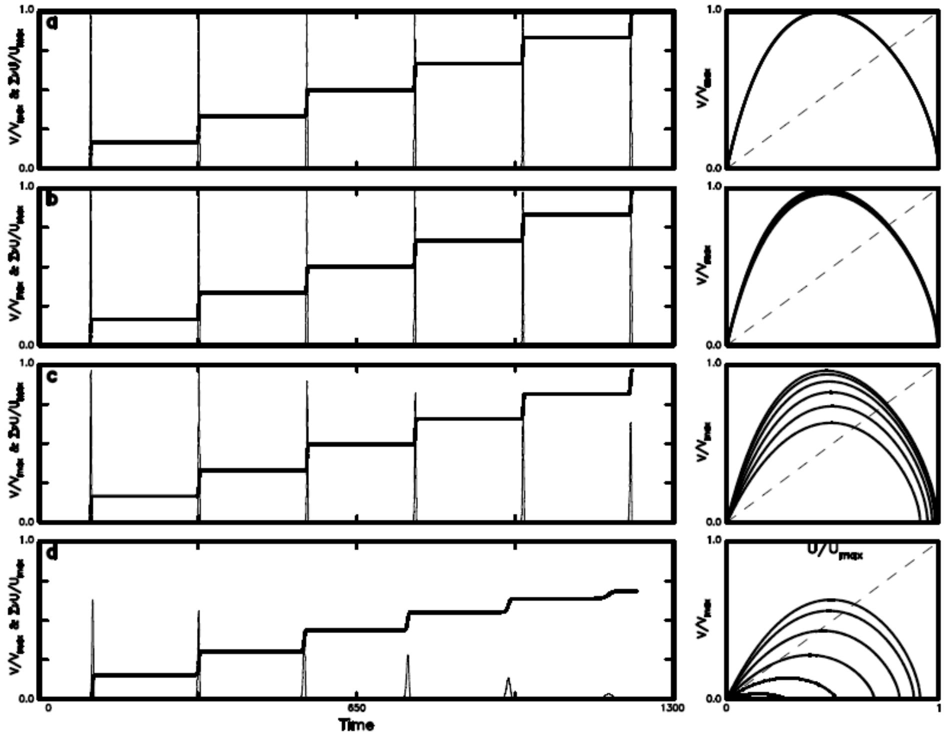

Figure 11. The time variations in V/V_{max} (thin solid line) and cumulative slip $\Sigma U/U_{max}$ (solid line) and the phase portrait of V/V_{max} versus U/U_{max} (solid line) for four values of C: (a) for C=0.0001; (b) for C=0.0010; (c) for C=0.0100; and (d) for C=0.0380 when U_{co}=0.1 and η=1.

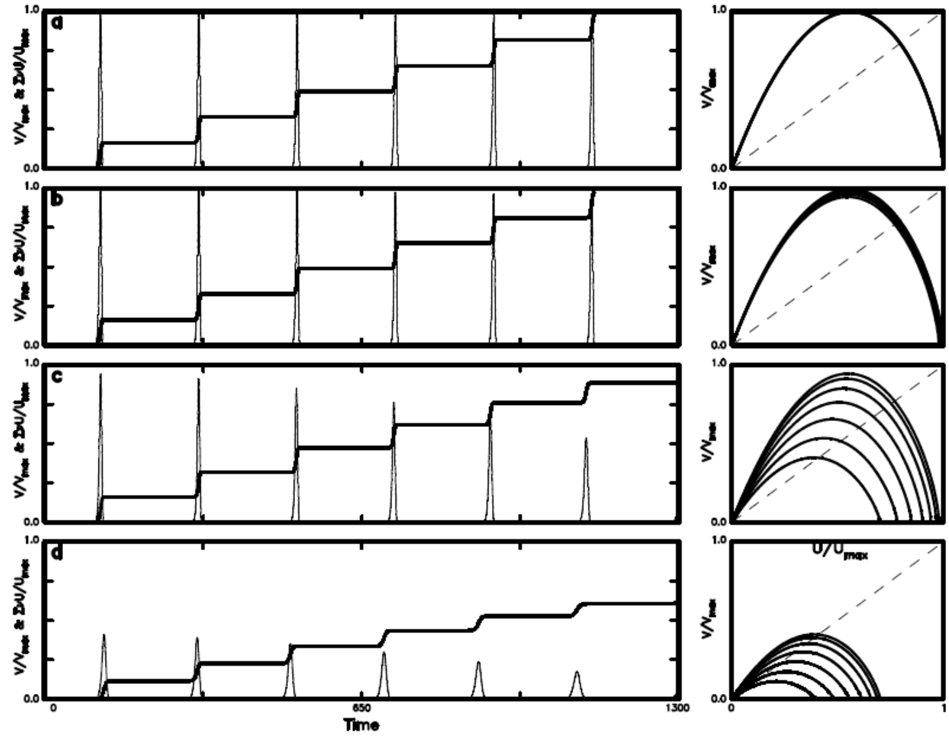

Figure 12. The time variations in V/V_{max} (thin solid line) and cumulative slip $\Sigma U/U_{max}$ (solid line) and the phase portrait of V/V_{max} versus U/U_{max} (solid line) for four values of C: (a) for C=0.0001; (b) for C=0.0010; (c) for C=0.0100; and (d) for C=0.0136 when U_{co}=0.5 and η=1.